The Pennsylvania State University
The Graduate School
Department of Engineering Science and Mechanics

PERFORMANCE DEGRADATION OF PCBM:P3HT POLYMER/FULLERENE PHOTOVOLTAIC CELLS UNDER GAMMA IRRADIATION

A Thesis in
Engineering Science
by
Aaron M. Todd

Submitted in Partial Fulfillment
of the Requirements
for the Degree of

Master of Science

December 2009

The thesis of Aaron M. Toddwas reviewed and approved* by the following:

Jian Xu
Associate Professor of Engineering Science and Mechanics
Adjunct Professor of Electrical Engineering
Thesis Co-Advisor

Osama Awadelkarim
Professor of Engineering Science and Mechanics
Thesis Co-Advisor

S. Ashok
Professor of Engineering Science and Mechanics

Judith Todd
Professor of Engineering Science and Mechanics
P.B. Breneman Department Head of Engineering Science and Mechanics

* Signatures are on file in the Engineering Science and Mechanics office.

Abstract

The gamma radiation damage effect on polymer-based hybrid photovoltaic cells consisting of a blend of poly-3-hexylthiophene (P3HT) and [6,6]-phenyl-C61-butyric acid methyl ester (PCBM) is investigated. The device is a bulk heterojunction photovoltaic cell with aluminum and ITO electrical contacts. Each glass substrate contains 6-to-9 usable devices. The samples were exposed to a cesium-137 gamma ray source (661 KeV) with radiation doses ranging from 1 krad to 5 krad.

Electronic characterization by current-voltage (I-V) measurements were carried out before and after exposure. Decreases in the short-circuit photocurrent and the filling factor (FF) are observed with increasing radiation doses. Charge transport characterization was completed by the use of the integral-mode time-of-flight (I-TOF) technique and the current extraction by a linearly increasing voltage (CELIV) technique. Decreases in the charge carrier mobility are observed for both techniques with the increasing radiation dose. The CELIV results also show a decrease in the extraction current maximum and the post-extraction displacement current ramp. Optical characterization by the measurement of absorption and photoluminescence spectra were carried out.

The results show that radiation exposure in the presence of oxygen strongly degrades the P3HT material. Damage in this material is in the form of polymer chain scission and conformational changes (twisting) which detrimentally affect the charge transport process inside the active layer.

Table of Contents

List of Figures

List of Tables

Acknowledgments

This research would not have been possible without the wisdom and experience of my advisor, Dr. Jian Xu, who helped steer the course of this project, and without the expertise and patience of my fellow graduate students, Alan Berger, Ting Zhu, and Fan Zhang, who sacrificed many hours sharing their research knowledge.

I also thank Mark Linsley, Radiation Safety Inspector of Penn State's Environmental Health and Safety Department, for his considerable help in facilitating the first radiation experiments for our group and conveying the knowledge of radiation necessary to begin this research. Finally, I thank Shailaja Hegde for her time and patience in operating the omnidirectional radiation source.

Chapter 1

Introduction

Photovoltaic cells have been utilized since the very early days of the space program development as a primary power source. Our increasingly complex network of satellites dedicated to communication, information broadcasting, space exploration and defense systems means that the need for these high-efficiency power sources will only continue to rise. Due to the rapid increase in demand for electronics-grade semiconductor materials over the last forty years, the microelectronics industry has become adept at the production of very high-purity silicon, gallium arsenide, germanium and other semiconductor material systems. The widespread availability of silicon and the continual research into the optimization of the device performance has led to large increases in the efficiency of silicon photovoltaic cells from 6% to 24% [1, 2]. Compound semiconductor systems have also received much attention, due to their relatively high power efficiencies and high radiation tolerance. Copper indium gallium selenide cells offer approximately 20% efficiency [3]. Gallium arsenide cells have even higher efficiencies and have been studied extensively for radiation hardness[4, 5] in space applications where power demand is high. Yet, there still remains the problem of high material cost and high fabrication cost for inorganic photovoltaics.

Any photovoltaic cell that is space-bound will be subjected to high-energy radiation above the Earth's atmosphere due to the Van Allen belt. The Van Allen belt is a series of radiation bands that surround the Earth and contain high-energy protons and electrons[6]. The particles are trapped in the Earth's magnetic field from storm activity, volcanic activity and deep-space cosmic rays. It is split into two distinct belts characterized by the particle type and energy present in each. The inner belt contains very high-energy protons (above 100 MeV) and electrons

of several hundred keV. It extends from approx. 500 km to 10,000 km above Earth. The outer belt, extending from approximately 20,000 km to 45,000 km, contains high-energy electrons (0.1-10 MeV). Under a typical circular or geosynchronous orbit, the electron flux will account for the majority of the radiation dose received by the satellite [7]. Within this belt, the particle flux, direction and intensity are continually fluctuating and spacecraft are bombarded with 1 million to 10 billion particles per square centimeter per second. The radiation doses absorbed at these altitudes remain the ultimate real-world radiation exposure that any photovoltaic system will be exposed to. It is therefore of great importance to understand the mechanisms by which high-energy radiation will damage next generation photovoltaic materials if there is the potential to be used in space applications.

The damage properties of a number of inorganic photovoltaic systems in these high radiation intensity environments are well understood [8, 9, 10, 11, 12, 13, 14, 15, 16, 17, 18] due to the long standing use by the space exploration program. However, rigid photovoltaic systems bring about logistical difficulties related to the deployment into space. The cells used presently require a mechanical system to carefully actuate the folding and unfolding of the cells to form a large array complete with electrical contacts. This introduces complexity, cost, and weight to the system, in addition to the cell material and fabrication costs. There is much demand for a more easily stowable power generation system that can solve these problems.

Organic, polymer-based photovoltaic cells have been attracting increasing research interest over the last two decades due to the ease of fabrication, low production cost, and the possibility to be used on flexible substrates. Fabrication of organic cells can be achieved by the use of low temperature spin- and dip- coating systems, and larger throughput roll-to-roll printing processes have been proposed[19]. Due to the ease of fabrication, it is envisioned that one day these photovoltaic materials can cheaply be cast onto large panes of window glass and unused roof space to act as a power generator[20]. The utilization of these organic cells in space is indeed very distant, but the major promise is the efficient stowing and deployment strategies that flexible substrates make possible. It is envisioned that large areas of this type of cell will be produced in a roll and transported up to orbit in a very compact, lightweight configuration where they can simply be unrolled. Studying the damage characteristics under gamma irradiation may also prove that these inexpensive materials are useful for cheap, sacrificial dosimetry devices. The organic cells cannot currently exceed or even meet the power-conversion efficiencies of inorganic systems,

but there have been a number of breakthroughs in recent years that have led to efficiencies as high as 4%[2]. Lower efficiency will still be useful if the device lifetime and overall cost of production are further optimized. Though there is reason to believe that research will continue to yield higher efficiencies for organic photovoltaics, there is still a great deal that is unknown about the performance of these cells in high radiation environments.

1.1 Objectives

This research required two main objectives in order to complete.

The first objective was to locate a suitable radiation source on campus that could be operated safely. Because this is the first use of gamma radiation in a device study experiment for our group, I was tasked with developing an understanding of the foundations of radiation science, specifically the types and energies of radiation, the various measurement techniques, and the safety of working with radiation. The Environmental Health and Safety Department of Penn State was instrumental in helping me to find a radiation source and explaining the safe operation of such a device. A multitude of preliminary experiments were carried out from September 2008-March 2009 using some of the initial test samples in an effort to gain some insight into the effect of radiation on our devices. These experiments were very crude and did not yield important results. However, those early tests gave a lot of insight into how radiation interacts with electronic materials and directly led to the design of the experiment herein.

The next objective of this research was to characterize the performance of a specific, high-efficiency organic photovoltaic cell after exposure to high-energy gamma radiation. The photovoltaic system is a phase-separated semiconducting polymer/fullerene derivative blend consisting of poly(3-hexylthiophene) (P3HT) and [6,6]-phenyl-C61-butyric acid methyl ester (PCBM). The material is sometimes referred to as a hybrid nanophase semiconductor due to the quasi-crystalline structure that self assembles in the active layer. The first step in accomplishing the objective was to fabricate a series of high-quality samples and verify their nominal performance. The characterization of these samples was by electronic testing methods to determine several conduction properties. A cesium-137 gamma radiation source, emitting electrons at 661 keV, was used to irradiate the samples, afterwhich further electronic testing was conduct to compare the results to the unexposed samples. The optical characterization was carried out by measure-

ment of the absorption spectra and the photoluminescence (PL) spectra, both of which reveal key information about the morphology of the active layer.

1.2 Design Requirements

The Photonic and Optoelectronic Devices Group is committed to understanding the physics of optoelectronic devices and optimizing their performance. Over several years a few of our group members have become experts on fabrication of the latest, high-efficiency organic polymer photovoltaic cells in addition to breakthroughs in the study of organic light-emitting diodes, biosensor devices, and nanoscale lasers that utilize semiconducting quantum dots. The design of my experiment required collaboration from each of the group members, meetings with radiation experts, extensive literature review and analysis time.

At the time of this writing, this research appeared to be the first damage study of the P3HT:PCBM system to utilize gamma radiation. Previously, one group had studied the same material using an X-ray source[21]. Because of the much higher particle energies of gamma radiation, it was uncertain how quickly significant damage to the device performance would be observed. Radiation dose rates and overall dosage were chosen in an effort to maximize the experiment time efficiency and yield results that show a good trend in the radiation damage to the devices. As such, the results do not show complete destruction of the performance of the devices, but rather useful information about the performance degradation trend that occurs with an increasing exposure to high-energy gamma radiation.

In order to be considered as a material for use in dosimetry devices, an efficient and reliable metric is needed to analyze the absorbed radiation dose. One study focused on the use of the degree of quenching to the PL spectra as a means of radiation detection[22]. Here, Zhong, *et al.*, use a high atomic number BiI_3 compound dispersed in poly[9-hexyl-9-(2-ethylhexyl)-fluorene-2,7-diyl] (HEH-PF) conjugated polymer. The BiI_3 serves as a gamma radiation sensitizer and alters the PL spectra according to the radiation dose. Though the P3HT:PCBM does not possess quite a high gamma radiation stopping potential as the high atomic number elements, the degradation of the PL spectra shows potential to be utilized as the mechanism for dosimetry applications.

Chapter 2

Literature Review

This chapter will detail background information that is relevant to this research. First, a timeline of the development of high-efficiency organic photovoltaic cells will be presented. Next, device physics pertaining to the P3HT:PCBM system will be outlined. Finally, a summary will be presented of other experiments with radiation and organic photovoltaic.

2.1 Organic Photovoltaics

2.1.1 Basic Operating Principles

The operation of any photovoltaic devices requires that incoming photons generate excitons (bound and mobile excited electron-hole pairs) and that these excitons can diffuse to a site where charge separation occurs, at which point the free charge carriers are extracted from the device. Inorganic photovoltaic systems achieve this by the p-n junction, whereby a semiconductor doped to have an excess of electrons and a semiconductor doped to have an excess of holes are brought together. A depletion region forms, as shown in Figure 2.1, and thus provides the built-in potential that is the driving force for the dissociation of photo-generated excitons and the extraction of current from the cell. Organic polymer materials are not intrinsically suited for this application, but initial studies were aimed at using certain intrinsically hole-conducting polymers in attempt to realize their photovoltaic effect.

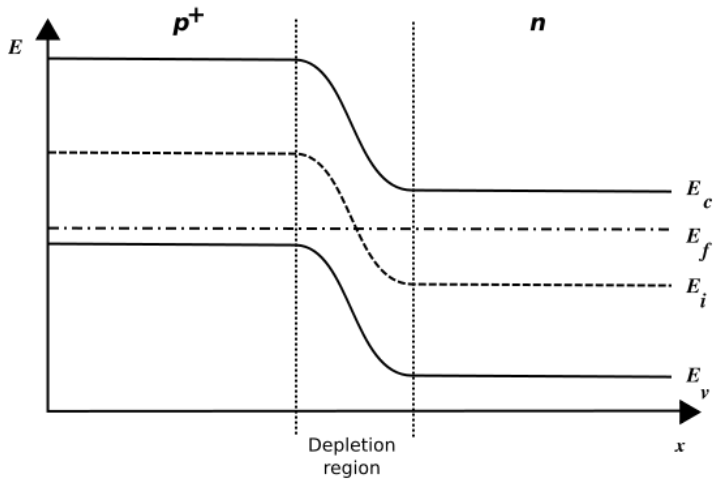

Figure 2.1. The band structure of a generic p-n junction

2.1.2 Homojunction

Early devices were fabricated as a pure polymer sandwiched between two metal contacts with differing workfunctions. The hole-conducting (p-type) polymer layer forms a Schottky barrier with the lower workfunction metal[23] and thus there is a built-in potential arising from the assymetry of the contact workfunctions (Figure 2.2). The photovoltaic efficiency of this configuration is low, however, because the difference between the workfunctions of the contacts must be substantially high to generate a large enough buit-in potential to reliably convert excitons into free carriers [3, 24]; only a small percentage of the excitons are disassociated before they recombine by luminescence or thermalization. Practical use of such cell configurations was severely limited due to efficiencies below 0.1% [2, 3, 23]. Some were able to realize efficiences from 0.7% to 1.0% with merocyanine dyes and the addition of an oxide layer on one of the metal contact layers[25, 26].

2.1.3 Single Heterojunction

The heterojunction structure device was a significant improvement over the homojunction device. Analogous to the p-n junction, it is composed of a hole-conducting polymer and an electron-conducting polymer that are stacked together in a layer structure. The heterojunction will have

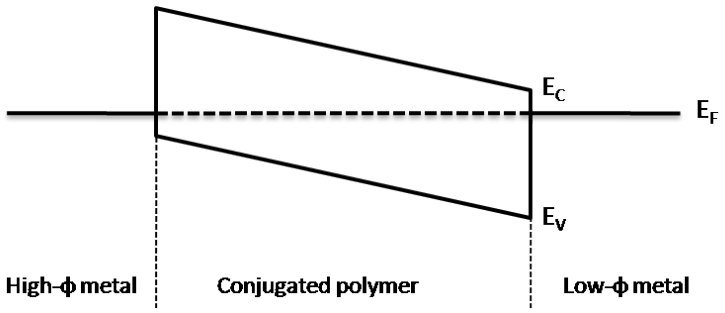

Figure 2.2. The band structure of a metal-insulator-metal diode.

an electronic band structure that better facilitates the dissociation of excitons due to a much higher built-in potential at the interface[20](Figure 2.3). However, the performance of early heterojunction cells was limited by two factors. First, the device thickness needs to be large enough to allow for substantial optical absorption. In direct competition with this requirement is a constraint on the device thickness due to exciton diffusion. The device thickness must be less than the excitonic diffusion length so that excitons can reach the charge separation interface before recombining thermally[27]. For a number of years the 1.0% efficiency reported by C. W. Tang[28] for a bilayer of copper phtalocyanine and a perylene tetracarboxylic derivative was the highest. Further improvements in organic photovoltaics occurred only after two important breakthroughs: the study of conjugated polymers and the realization of photo-induced, ultrafast charge transfer.

2.1.4 Conjugated Polymers

Conjugated polymers of the poly(3-akylthiophene) family have been utilized as photoresists, light-emitting diodes, electrochromic materials, microwave absorbers, electrostatic coatings, electromagnetic shields, optical modulators and transistors[29, 30, 31, 32]. For photovoltaic applications they originally came under research because of the very high optical absorption coefficients that are possible[2, 27]. They are characterized by delocalized electrons, due to the overlapping of the π-orbitals along the polymer backbone, which causes an extended π-system to form(Figure 2.4). This results in a filled valence state and a small electronic bandgap. Bandgaps for conjugated polymers are typically greater than 1.8 eV, and as such, do not absorb near as much of the solar

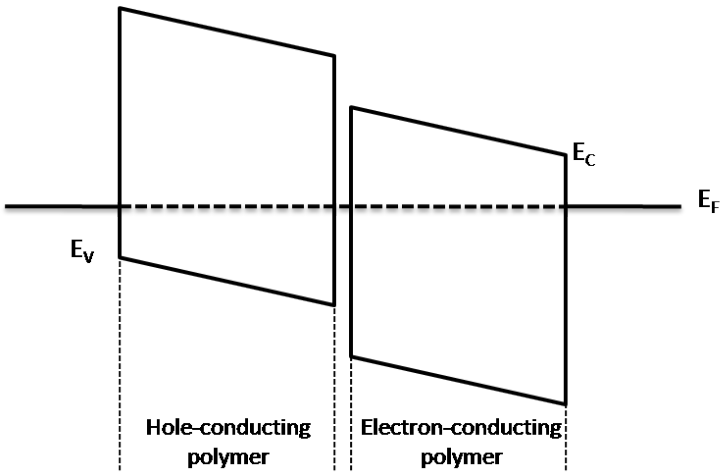

Figure 2.3. The band structure of a heterojunction with donor and acceptor polymers.

spectrum as silicon with its bandgap of 1.1 eV[33]. However, the organic materials have very high optical absorption coefficients, up to 10^5 cm^{-1}, so it is possible to use very thin devices of 100 nm and still achieve respectable device performance[23, 27, 33].

2.1.5 Ultrafast, Photo-induced Charge Transfer

Perhaps the most important discovery in the study of organic photovoltaics was the ultrafast, photo-induced charge transfer process discovered by Sariciftci and coworkers[24]. This phenomenon was discovered whilst studying a composite structure of MEH-PPV and the Buckminsterfullerene molecule. The Buckminsterfullerene molecule (C_{60}) is a strong electron acceptor and essentially forms a p-n junction with a high built-in potential when in contact with the conjugated polymer. Evidenced by the complete quenching of the photoluminesce spectrum of the polymer, excitons forming in the composite were rapidly charge separated at the polymer/fullerene interface before any other relaxation processes could occur. Further work revealed that this charge transfer process occurs in a time of ˜45 fs[34].

2.1.6 Bulk Heterojunction

The realization of the ultrafast, photo-induced charge transfer process directly led to the study of the bulk heterojunction. The bulk heterojunction is formed by an interpenetrating, phase-

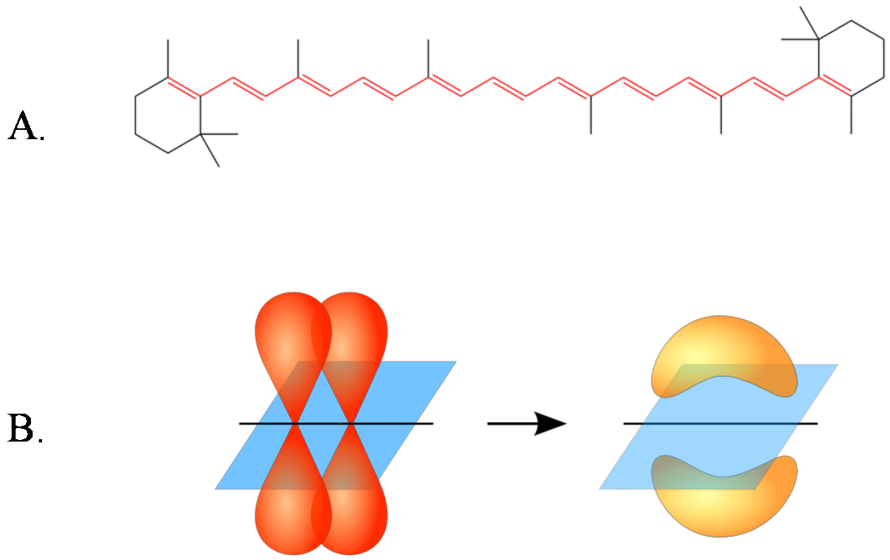

Figure 2.4. (a) the alternating single and double p-bonds on beta carotene and (b) the overlapping π-orbitals which give rise to the delocalized electron system.

separated donor-acceptor composite. The morphology of this configuration results in a vastly increased interaction area between the donor and acceptor species as compared to a single heterojunction structure[20]. The Buckminsterfullerene has a limited solubility[27], but a suitable fullerene derivative with higher solubility was found in the form of PCBM[35]. The PCBM molecule automatically forms a crystalline structure within the polymer matrix due to its spherical geometry[36] and the distances between charge-separation sites are on the order of the exciton diffusion length[3, 27]. A schematic of the charge transfer process between the P3HT and PCBM molecules is shown in Figure 2.5 [37]. The fact that the charge transfer process dominates all other exciton relaxation processes and that excitons form within one diffusion length from a charge-separation site equates to an internal quantum efficiency of nearly 100%[24, 38].

2.2 Radiation and Organic Photovoltaic Cells

There is not a widespread understanding of the radiation damage to organic cells at present. The prospect of utilizing organic cells in space or for dosimetry applications necessitates the study of

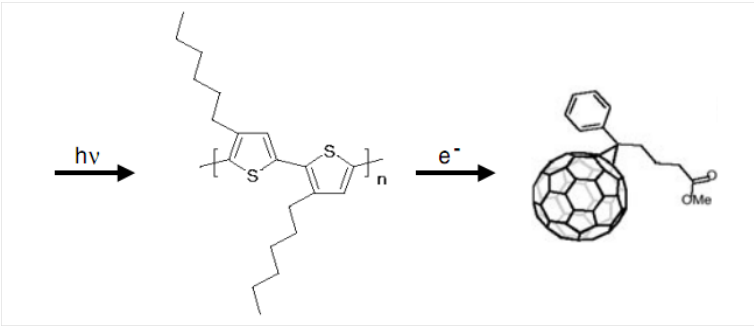

Figure 2.5. The charge transfer process from individual molecules of P3HT to PCBM.

the radiation damage characteristics.

A previous study of the P3HT:PCBM system has been conducted by Li, *et al.*, to investigate the radiation induced damage by x-rays[21]. They have exposed samples with a similar structure as ours to a tungsten x-ray source operating at a dose rate of approximately 8.33 krad per minute. Over a time period of 60 minutes, they report degradation of the power conversion efficiency from 4.1% to 2.2%, corresponding to a dose of 500 krad. They observed a reduction in the open-circuit voltage (V_{oc}) to 91% of the unirradiated value. Li, *et al.*, have also studied the recovery effect on the cells for a period of 240 minutes after exposure and found that the cells recovered, on average, to 2.9% power conversion efficiency and 93% of the unirradiated value of V_{oc}.

The notable differences between the study by Li and our study are the type of radiation and the direct measurement of the mobility properties. Despite a significantly lower photon flux, the individual photon energies from the gamma radiation source are 5-10 times higher at 661 keV. These higher energies will result in unique results. Furthermore, in the study by Li the parameter of the carrier lifetime-mobility product ($\mu\tau$) is extracted from I-V curves by a curve fitting procedure, whereas in our study we will use two different charge transport experiments to directly analyze the mobility of the carriers in the samples.

Chapter 3

Experimental Details

3.1 Sample Fabrication

Each sample is fabricated on a 1 in^2 indium tin oxide (ITO) glass substrate. ITO serves as the transparent anode connection to the active layer. In a series of 15-minute stages the substrates are cleaned in a sonicator with detergent, deionized water, acetone, and isopropyl alcohol (IPA) for two stages each. The substrates are baked to remove any remaining solvents and exposed in an ultraviolet oven to make the substrate hydrophilic. A layer of the conducting polymer poly(4,3-ethylenedioxythiophene):poly(styrene sulfonate) (PEDOT:PSS) is spin-coated. PEDOT:PSS facilitates hole transport and improves the surface adhesion with the ITO layer [27]. At this point, samples are transferred into a nitrogen glove box for the remaining fabrication and any long-term sample storage. Next, the P3HT:PCBM mixture (1:1 by weight in chlorobenzene at 12 mg/mL) is spin-coated. The 1:1 ratio has been reported to result in a nearly balanced electron and hole mobility while minimizing recombination in the active layer[37, 39, 40]. The use of the chlorobenzene solvent has been found to result in a device that is more efficient due to enhanced interchain interactions in the polymer[41]. The sample is then annealed at 140°C for 30 minutes. Annealing has been shown to improve the device efficiency by recrystallizing the P3HT:PCBM layer, reducing the density of interface defects and improving interchain interactions [27, 42, 43, 44]. Finally, using the in-box thermal evaporator chamber, circular aluminum contacts of approximately 0.7 cm^2 are deposited onto the active layer to serve as cathodes, resulting in 6-9 photovoltaic devices per sample. Figure 3.1 shows the device structure.

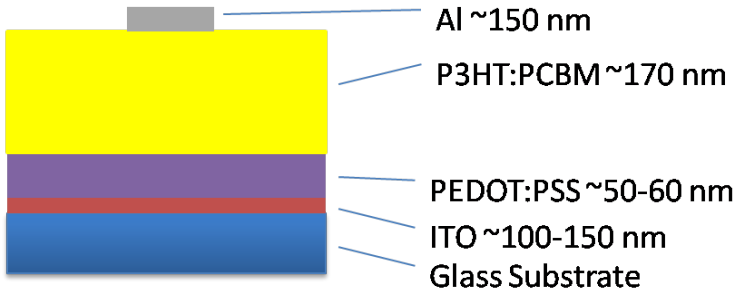

Figure 3.1. The device structure of P3HT:PCBM photovoltaic cells.

The nitrogen glove box is a non-volatile environment that eliminates oxygen reactions that can lead to defects in the devices. It is also a low dust environment because of the purifier system which continuously filters the air. During transport to the radiation exposure site and during electronic measurements the samples were exposed to the oxygen environment, and there have been concerns over the ambient degradation effect of oxygen on the device performance, as semiconducting polymers have been found to degrade in oxygen[45]. However, research has shown that the addition of the fullerene structures enhances the stability of the active layer in oxygen and, the formation of positive polarons on the polymer chain substantially reduces the reactivity of the polymer with oxygen[46]. A specific study of P3HT:PCBM has shown that the timescales necessary to observe 80% degradation of their device performance was on the order of 1000 hours [47]. This far exceeds the oxygen exposure times incurred in our study during transportation. However, as discussed further in Chapter 5, the presence of oxygen during the radiation exposures is found to play a large role in the damage mechanism to P3HT:PCBM.

3.2 Radiation Exposures

The radiation source used in our study is an omnidirectional gamma radiation source. The sample is placed in a sample holder on a rotating stage at the center of the lead chamber with approximately 28,000 cm^3 internal volume. The source is a cesium-137 source (661 keV) and is introduced into a corner of the chamber. The chamber allows radiation to reflect from the walls and interact with the sample from all directions. The system is equipped with an automated

calibration system to deliver a specific radiation dose to the sample present in the chamber. A schematic of the sample is shown in Figure 3.2.

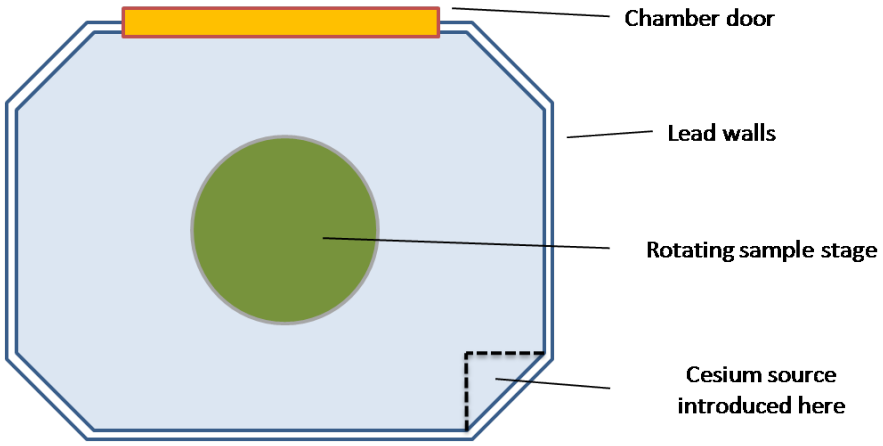

Figure 3.2. Schematic of the omnidirectional gamma radiation source

The samples were irradiated by exposure to the cesium-137 source at a dose rate of approximately 1 krad/min for times required to obtain total radiation doses of 1 krad to 5 krad for 5 samples. The control sample was not exposed to radiation but was brought to the exposure site to ensure that it experienced the same oxygen-exposure time outside of the nitrogen glove box as the test samples.

3.3 I-V Curve Experiment Setup

All current-voltage measurements were conducted using a Keithley 4200 Semiconductor Characterization System. A grounding clip was connected to the sample so that it contacted the ITO anode layer, and a copper wire probe was touched to the aluminum cathode as a soft contact. The voltage was swept from -1.2 V to +1.2 V in increments of 10 mV. The short-circuit current (I_{sc}) and open-circuit voltage (V_{oc}) parameters were extracted from the curves and used to analyze the performance. The I-V curve measurement setup is shown in Figure 3.3.

Following the sample fabrication, representative I-V curves were taken in laser-illuminated conditions (532 nm) for all devices on the control sample and the 5 test samples to establish the baseline performance. Post-irradiation, I-V curves were measured again in the laser-illuminated

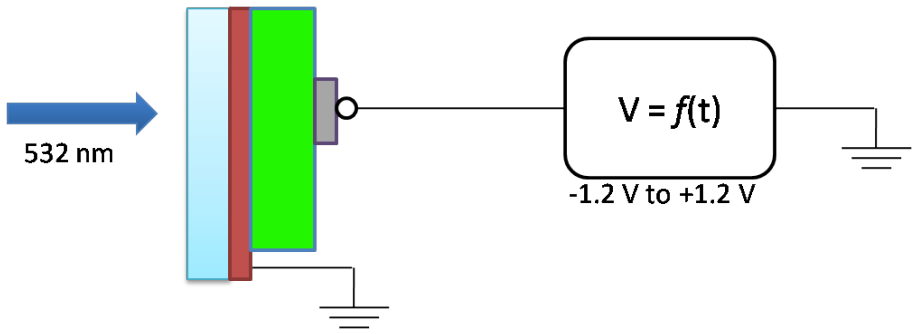

Figure 3.3. Schematic of the current-voltage curve measurement setup.

conditions for all samples.

3.4 I-TOF Experiment Setup

One method of measuring the charge carrier mobility is by time-of-flight (TOF) techniques. The simplest TOF measurement is the so-called "'current-mode"'. A bias voltage is applied to the thin film sample, and a laser pulse is used to generate a sheet of charge carriers. The bias causes the charge carriers to separate and travel to their respective electrodes. From the resulting current transient the carrier transit time (t_{tr}) can be extracted and the carrier mobility (μ) can be calculated from Eq. 3.1:

$$\mu = \frac{d^2}{V \times t_{tr}} \tag{3.1}$$

The current-mode TOF is not suitable in the case of our devices for two main reasons. First, carrier transient time must be substantially longer than the RC time constant of the measurement system in order to yield accurate results [48, 49]. Also, the sample must absorb the incident light pulse completely, with most of the absorption occurring near the transparent electrode. In both cases, a sample thickness on the order of several microns is necessary. For this reason the integral-mode TOF (I-TOF) technique is better suited to our thin film devices (˜170 nm active layer). It can also be said that I-TOF is suitable for subnanosecond transport properties due to measuring the collected charge rather than the current flow [50].

The integral-mode time-of-flight (I-TOF) works by measuring the charge collected on a capacitor after the sample has been biased and excited by laser. An initial bias potential is applied to the sample to remove any residual free charge carriers as well as to positively charge the output capacitor. The laser pulse occurs very shortly after the rising edge of the voltage pulse and causes the generation of excitons at the transparent contact. The built-in potential of the bulk heterojunction dissociates these excitons and the electric field sweeps the free electrons across the sample. When the electrons combine with the positive charge carriers at the cathode they cause a reduction in the initial charge on the capacitor, which is observed as a voltage transient on the oscilloscope. The initial slope of the voltage transient is used to calculate t_{tr}. Details of this calculation will be shown in Chapter 4. The I-TOF experiment setup is shown in Figure 3.4. The light source is an Nd:YAG laser (532 nm and 1064 nm) with a 10 ns pulse width and 10 kHz repetition rate. The infrared and visible portions of the laser output are separated by the method shown in Figure 3.5. The 5 V bias pulse is triggered by the infrared portion of the Nd:YAG laser and a digital delay generator. The pulse is triggered with adequate delay so that it actually starts just before the next laser pulse, with a time around 1 μs between bias application and laser pulse. The method for contacting the sample anode and cathode is the same as that described in the I-V curve measurement setup.

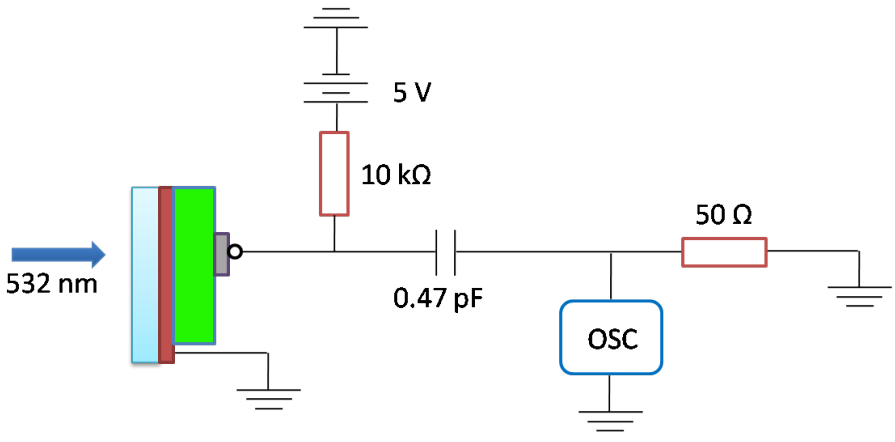

Figure 3.4. Schematic of the integral-mode TOF measurement setup.

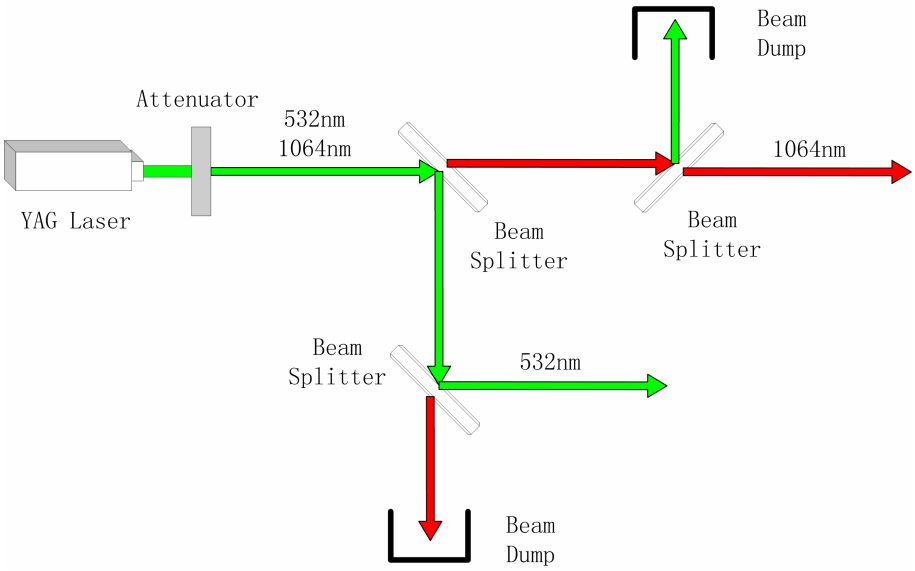

Figure 3.5. Separation of the Nd:YAG laser output

3.5 CELIV Experiment Setup

There are several problems which come about when using the TOF techniques for the study of the thin film organic cells due to the heterogeneous microstructure and relatively high dark conductivity of P3HT:PCBM[51]. The assumption by TOF that the electric field is uniformly distributed is violated. Contact capacitances that are higher than the geometrical value are observed even in high-frequency measurements, suggesting that the electric field is concentrated on the contact region, and carriers do not move through the total thickness of the active region. In this regard, mobilities can be overestimated when the full sample thickness is used in calculations. Furthermore, the backward movement of photogenerated electrons cannot be ruled out in materials with relatively large light absorption depths.

The technique of current extraction by a linearly increasing voltage (CELIV) has been developed to mitigate these concerns for the study of charge transport properties in organic semiconductors. The equilibrium carrier extraction is measured, rather than the photogenerated carriers, as in TOF. It has been proposed that the CELIV technique is more accurate than TOF for measuring the extraction time [48]. The application of the linearly increasing voltage initially yields a uniform electric field. There is the formation of a charge-depleted region on the opposite

side of the sample because of charge unscreening as carriers are extracted from the sample. In the depletion region there remains a linearly decreasing field which gradually expands to fill the entire active layer as charges are swept away. At a time t_{max} the depletion region now consumes the entire thickness of the sample and a maximum current output transient is observed. The maximum corresponds to the time at which equilibrium charge carriers have been extracted from the full sample thickness.

There are three cases where mobility can be evaluated by CELIV: (1) high conductivity, (2) low conductivity, and (3) moderate conductivity. For the purpose of this study the moderate conductivity case is used and the Equation 3.2 is applied, where A is the linearly increasing voltage slope U/t_{pulse}, d is the active layer thickness, Δj is the current extraction due to conductivity, and $j(0)$ is the displacement current due to sample capacitance:

$$\mu = \frac{2 \times d^2}{3At_{max}^2(1 + 0.36\frac{\Delta j}{j(0)})} \tag{3.2}$$

The current output transient has several features. When the linearly increasing voltage is first applied the output transient very rapidly increases to the displacement current, due to sample capacitance[52]. The output transient will gradually increase from this value until the extraction time t_{max} is reached. The output transient then drops until it reaches the displacement current again. A schematic representative CELIV output transient is shown in Figure 3.6.

Systems that are undoped, or have a low concentration of equilibrium carriers can be studied by the photo-CELIV technique, where a laser pulse is used to stimulate charge carriers in the sample. Subtracting the photo-CELIV curve from the dark condition CELIV will yield information about the photogenerated charge carriers only, and varying the time delay between the laser pulse and linearly increasing voltage can be used to study the lifetime of the photogenerated charge carriers before recombination. The work of Pivrikas, *et al.*, reports on the study of the P3HT:PCBM system using both the CELIV and photo-CELIV technique[52]. They measured electron mobilities of $2\times10^{-4}\ cm^2/Vs$. The results showed that longer carrier lifetimes are present for P3HT:PCBM than for organic cells of MDMO-PPV:PCBM. Additionally, a very strong dependence was found between the carrier mobility and the film morphology due to preparation techniques. Minute differences in the fabrication process can often lead to orders-of-magnitude difference in the measured mobility values for polymer/fullerene systems.

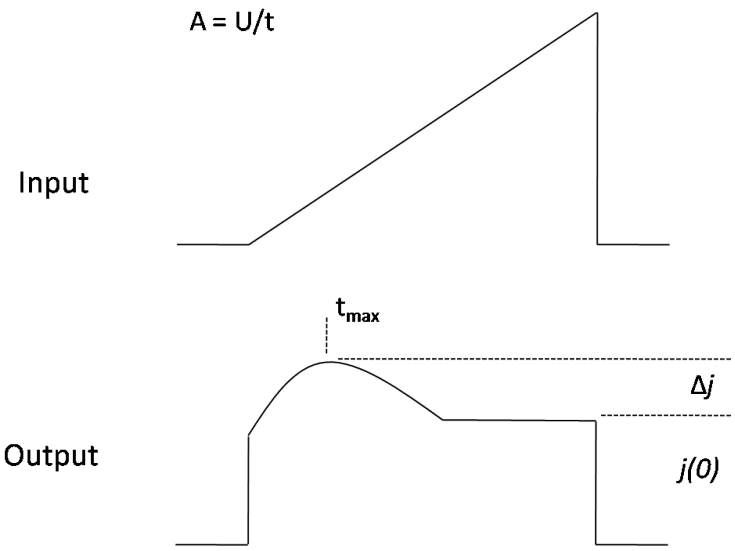

Figure 3.6. CELIV curve input and representative output with parameters of interest highlighted.

The most notable problem with the CELIV technique is the fact that it can only yield information about the majority carriers[51]. This leads to difficulty studying the P3HT:PCBM system because it has been specifically designed to have very similar electron and hole conducting properties. In the current output transient of non-balanced charge transport materials it will be possible to observe two current extraction peaks, whereas the two peaks will coincide for the study of P3HT:PCBM. It is for this reason that CELIV is used as a comparative tool in this study to look at relative degradation of carrier mobility due to radiation and not as a tool to calculate the exact mobility of electrons or holes. The experiment setup is shown in Figure 3.7. The method for contacting the sample anode and cathode is the same as that described in the I-V curve measurement setup. The sample is biased at -1 V and the linearly increasing voltage has an amplitude of 6 V with a duration of 20 μs. The output was measured on a digital oscilloscope in voltage-time mode.

3.6 Absorption Spectra Measurement

The absorption spectra is a characterization of the wavelengths of electrogmagnetic radiation that are absorbed by a material. The LAMBDA 19 UV-Vis-NIR spectrometer accomplishes this

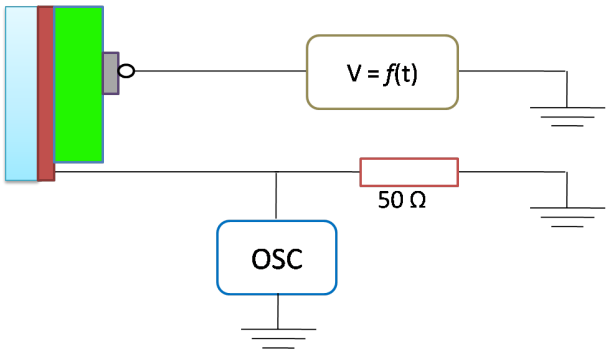

Figure 3.7. Schematic of CELIV measurement setup.

by focusing light of specific wavelengths onto the material and measuring the intensity of the light that is transmitted through. The absorption spectra is measured for the control sample and compared to the spectra for each of the radiation-exposed samples.

3.7 Photoluminesence Spectra Measurement

The photoluminesence (PL) spectra is a characterization of the light emission of a material. The material is stimulated with an excitation laser and a sensor detects the intensity of the emission as a function of the emission wavelength. The experimental setup is shown in Figure 3.8. Care is taken to minimize detection of the excitation wavelength (490nm) by using a 45 degree angle of incidence for the excitation laser. Additionally, only regions of the sample between devices are tested in order to eliminate reflection of the excitation laser from the backside of the aluminum contact. The strongest detection signal is measured with the optical fiber aligned perpendicularly to the sample surface and located in the region of the PL emission with the highest intensity. The signal is analyzed by the Ocean Optics HR2000 High Resolution spectrometer.

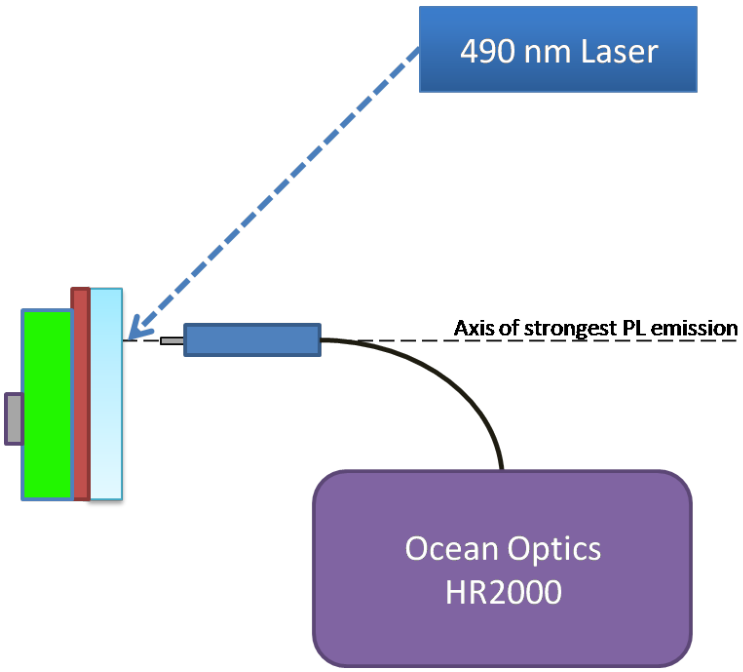

Figure 3.8. The Photoluminescence spectra measurement setup.

Chapter 4

Results

Presented herein are the results and analysis techniques for the I-V curve, I-TOF, and CELIV measurements. The purpose of these results is to gain insight into the degradation process that occurs in P3HT:PCBM as the gamma radiation dose is increased.

4.1 I-V Curves

Figure 4.1 shows the I-V curves corresponding to the different radiation doses. The most pertinent portion of the curves is shown, highlighting the change in short-circuit photocurrent (I_{sc}) and the open-circuit photopotential (V_{oc}).

A very clear reduction in I_{sc} is observed and representeded in Figure 4.2. However, there was no trend observed in V_{oc}.

The fill factor (FF) is calculated by finding the max value of $\frac{I \times V}{I_{sc} \times V_{oc}}$ for all points along the I-V curve. The FF is a ratio of the maximum attainable power of the photovoltaic cell to the theoretical maximum power. It is impossible to achieve the theoretical maximum power, but an FF of approximately 60%-70% is common for high quality silicon cells. Figure 4.3 shows the change in the FF as the radiation dose increases. The devices used in this study have a respectable starting FF of around 50%. We observe here that the cell device is able to retain a stable power generation from a standpoint relative to the overall decrease in I_{sc}. It is only at the 4 krad dose that significant alteration of the power generation ability is seen. Referring to the I-V curves shown above, the effect of a reduction in FF is a broadening of the curve inflection

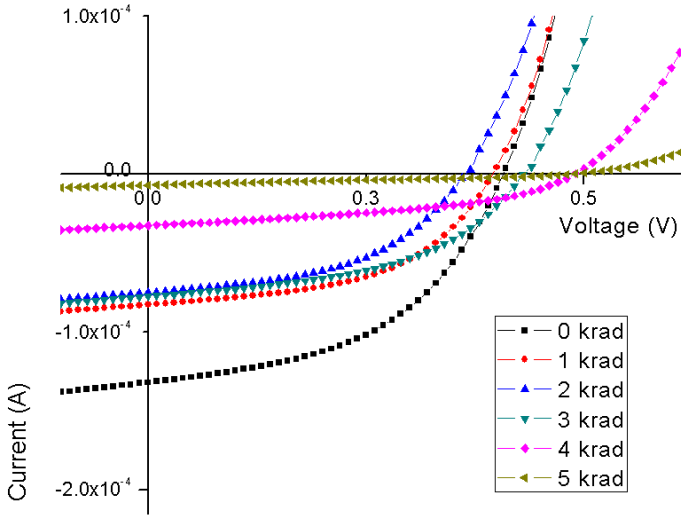

Figure 4.1. Pertinent sections of I-V curves under illumination.

between the I_{sc} and V_{oc} points, which is clearly noted for the 5 krad dose on the I-V curves.

4.2 I-TOF Measurements

A significant problem was found with the I-TOF results. The results suggest that there was substantial degradation of the samples by the time the experiment was conducted. The experiment was the last one conducted, and the samples had been in glovebox storage for approximately one month without usage. In previous experiments long-term storage in the nitrogen environment has proven to be quite stable, so one cannot completely rule out the possibility of experimental setup error and sustained damage to the sample contacts.

A particular source of difficulty in the past has been sample contact. The grounding clip must pierce through the active layer and PEDOT to make contact with the ITO. Care is always taken to adjust the grounding clip several times while comparing the signal strength to have confidence in the ground connection. A more likely source of contact problems is the aluminum

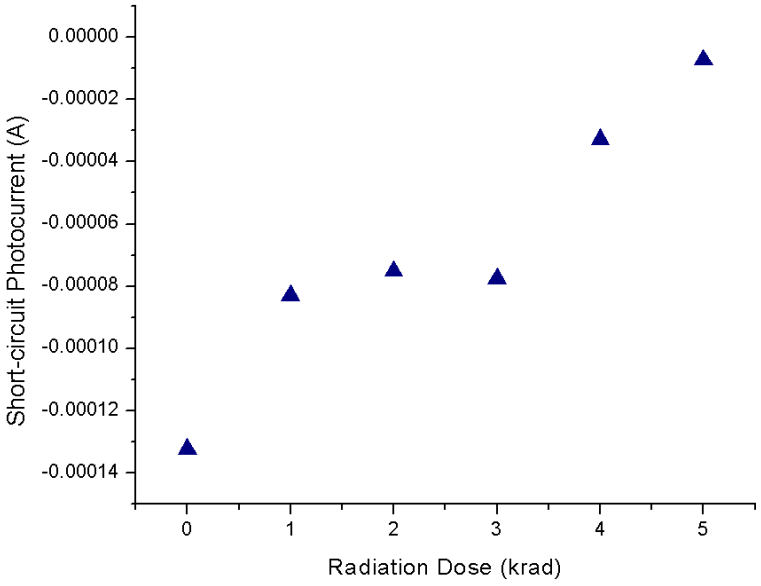

Figure 4.2. Short-circuit photocurrent versus radiation dose.

cathode. The copper wire probe has been continually maintained with new wire in the hopes of eliminating contact problems from the equipment side, but the aluminum on each device is still subject to mechanical stress from multiple series of tests. Some of the device contacts have small scratches that are visible with the naked eye, while other defects become obvious when the laser light breaches through microscopic defects that have formed in the contact. Careful use of the copper wire probe is critical to maintaining the integrity of these contacts, but some damage over time is unavoidable. Results from several of the devices on various samples had to be excluded due to this kind of error.

Typically, TOF mobility values for P3HT:PCBM are overestimated because of the non-uniformly distributed electric field in the sample. Due to the aforementioned sample degradation the mobility values found here are much lower than those in the literature. However, the results are still useful for observing the radiation effect, as the trend of decreasing mobility is clearly observed. A series of I-TOF signals is shown in Figure 4.4.

Analysis of an I-TOF signal involves extraction of the initial slope. A linear fit was used in the

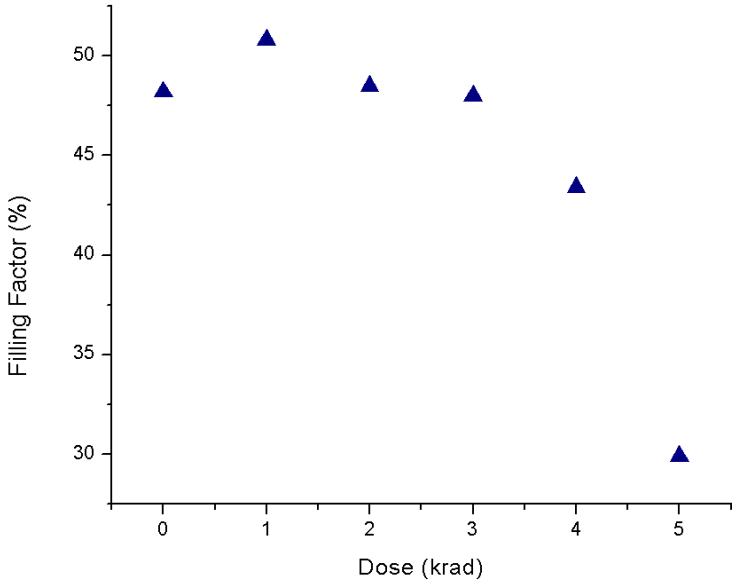

Figure 4.3. Reduction in calculated filling factor versus radiation dose.

Origin® graphing software and the slope value was obtained as shown in Figure 4.5. Because of this slope extraction step there is a small amount of uncertainty introduced into the calculations. This uncertaintly is not enough to affect results by orders of magnitude, so this cannot explain the lower than expected I-TOF mobilities. The value of slope is normalized with the applied voltage pulse to yield $\frac{d(\frac{U}{U_0})}{dt}$. The carrier transit time t_{tr} is then obtained by Equation 4.1:

$$t_{tr} = \frac{1}{2 \times \frac{d(\frac{U}{U_0})}{dt}} \tag{4.1}$$

Then, t_{tr} can be inserted into Equation 3.1 to yield the I-TOF carrier mobility.

The average carrier mobilities for each radiation dose are shown in Table 4.1. An increase in the carrier mobility is observed from the 2 krad sample to the 3 krad sample. There is no obvious explanation for the effect, but it is not something that is expected. This is observed in the CELIV measurement as well.

A broader look at the measured mobilities for each device gives a better picture of the degra-

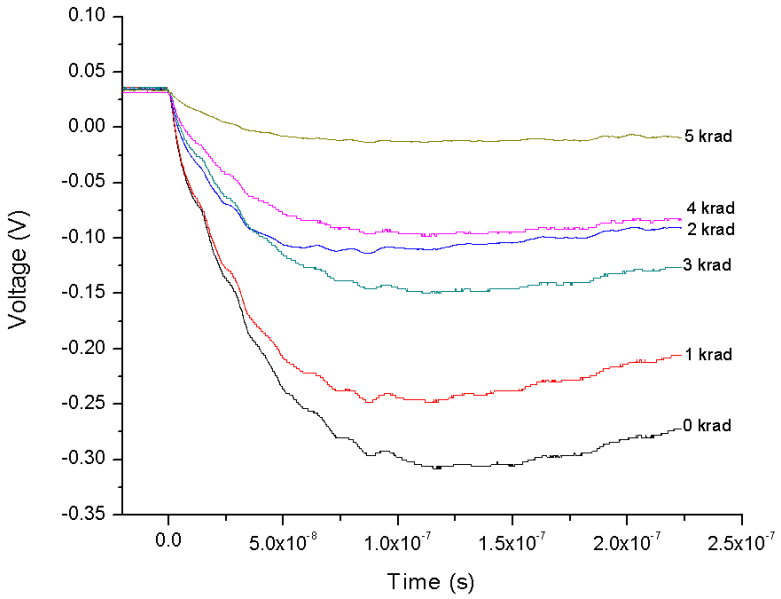

Figure 4.4. Comparison of I-TOF signals with increasing radiation dose.

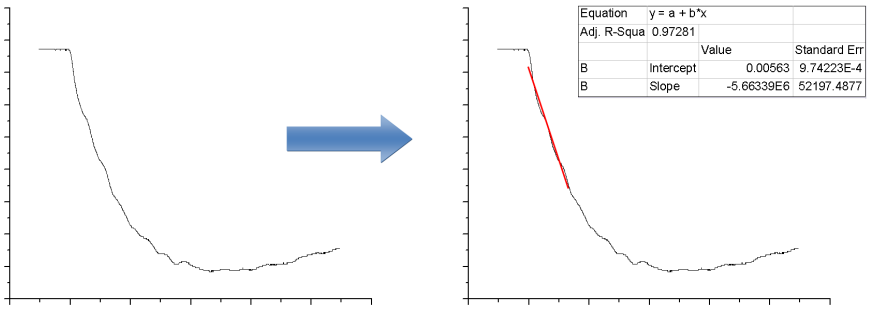

Figure 4.5. Linear fit and slope value extraction from I-TOF curve.

Table 4.1. Average carrier mobilities by I-TOF.

Dose (krad)	Mobility (cm^2/Vs)
0	1.182×10^{-5}
1	7.724×10^{-6}
2	6.120×10^{-6}
3	8.273×10^{-6}
4	7.498×10^{-6}
5	4.203×10^{-6}

dation trend, as seen in Figure 4.6. Here it is clear that there are some outlying samples that have either slightly better or slightly worse performance. This is likely due to the nature of solution-based fabrication. Spin-coating produces a fairly uniform thickness film but there will be small variations in the morphology and these variations can have an impact on charge carrier mobilities over as much as an order of magnitude[52].

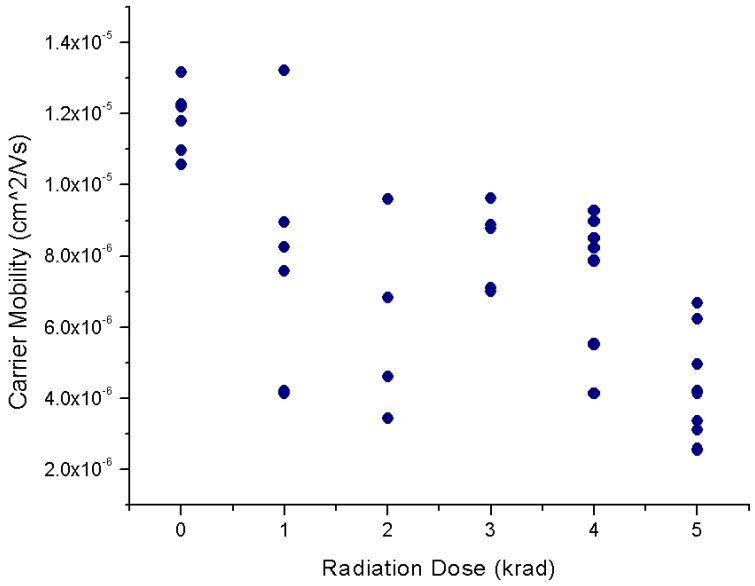

Figure 4.6. Measured carrier mobilities from I-TOF with increasing radiation dose.

4.3 CELIV Measurements

Overall, the CELIV measurements tend to be more consistent from device-to-device. The extraction of parameters from the CELIV transient involves less uncertainty, in addition to the advantages of CELIV over I-TOF that were described in Chapter 3. A representative CELIV curve is shown with highlighted parameters in Figure 4.7.

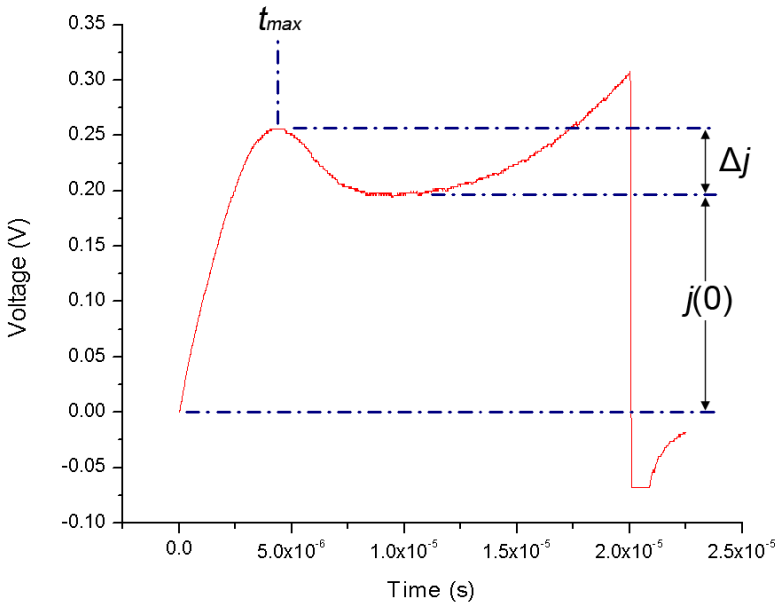

Figure 4.7. Actual CELIV curve for P3HT:PCBM showing the parameters of interest

The parameters t_{max}, $j(0)$, and Δj are used with Equation 3.2 to find the majority carrier mobility. The average calculated mobility values for each radiation dose are shown in Table 4.2.

Here we again see a small increase in the mobility from the 2 krad sample to the 3 krad sample. The much smaller difference in the mobility increase observed for CELIV suggests that the increase is, in fact, due only to small uncertainties introduced during fabrication and variation from device-to-device and is not an effect of transport physics specifically. The decreasing trend of mobility remains intact over the whole of the radiation doses.

Figure 4.8 shows the CELIV carrier mobilities for each radiation dose. The lower deviation

Table 4.2. Average carrier mobilities by CELIV.

Dose (krad)	Mobility (cm^2/Vs)
0	3.073×10^{-5}
1	3.013×10^{-5}
2	2.775×10^{-5}
3	2.811×10^{-5}
4	2.216×10^{-5}
5	1.785×10^{-5}

in values for each radiation dose confirms that CELIV is more consistent from device-to-device, and that there is less uncertainty introduced into the calculation than with the slope estimation required for I-TOF.

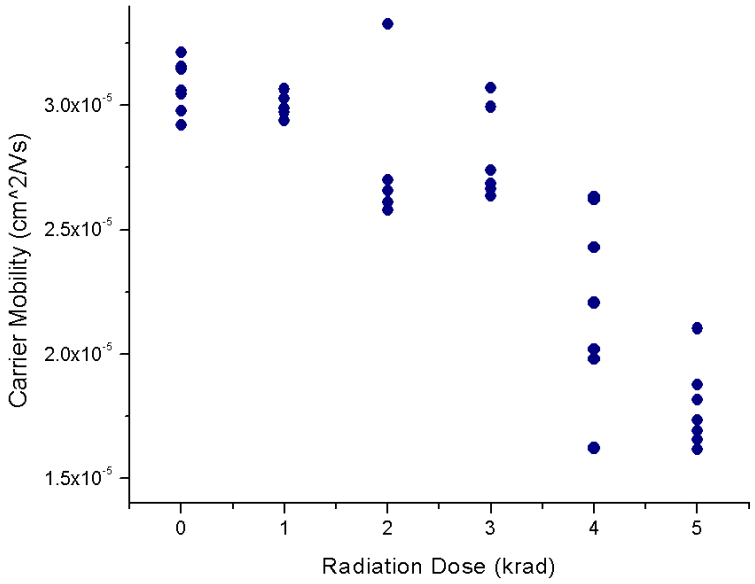

Figure 4.8. Measured carrier mobilities from CELIV with increasing radiation dose.

Comparing representative curves from each radiation dose shows interesting results. Figure 4.9 shows one device curve for each radiation dose, and two distinct trends are observed. First,

we see a decrease in the magnitude of the total extraction current at t_{max}. This is indicative of an overall reduction in conductivity of the device. However, if we compare Δj for each radiation dose there is no trend to increasing or decreasing. The lack of trend implies that the radiation damage affects the displacement current $j(0)$ and not the equilibrium carrier concentration that is extracted by Δj.

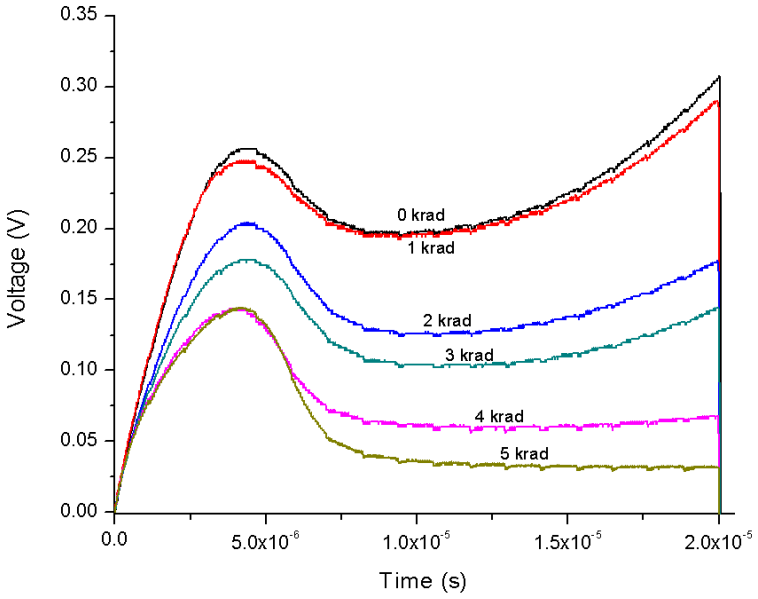

Figure 4.9. Changes in CELIV signal with increasing radiation dose

The second trend observed from the CELIV curves is a complete destruction of the post-extraction increase in $j(0)$, herein referred to as the displacement current ramp, as the radiation dose is increased. The reason for this trend is not obvious, but implies that there is some kind of leakage current brought about by the higher electric fields inside the sample at the tail of the input voltage transient. With a reduction in the displacement current ramp observed with radiation dose this means there is a change ocurring in the active layer that is impeding the generation of this leakage current.

4.4 Absorption Spectra

The absorption spectra for the irradiated samples are shown in Figure 4.10. There is no observed shift in the spectra peak and no substantial variation in the signal strength for each sample. This indicates that the degradation effects observed are not due to bulk changes of the material, but are more likely caused by highly localized defects in the material.

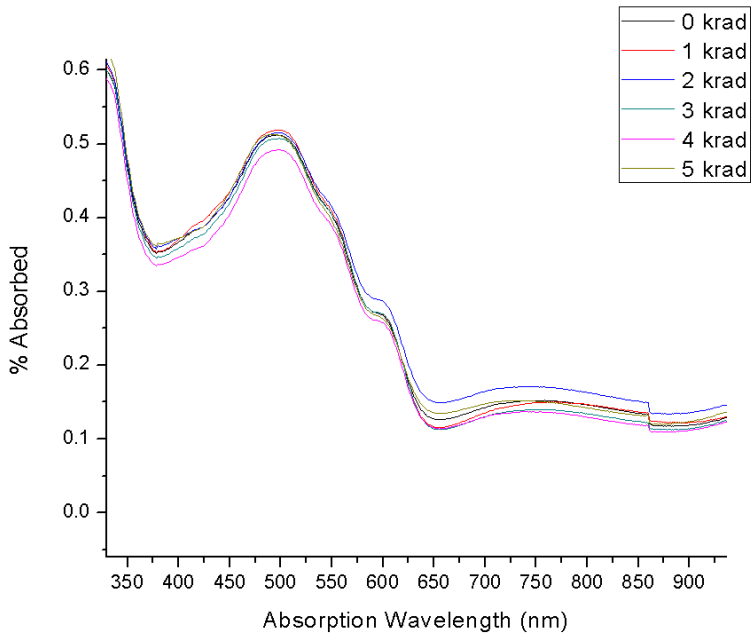

Figure 4.10. UV-Vis-NIR absorption spectra for each sample.

4.5 Photoluminescence Spectra

The photoluminescence (PL) spectra for the irradiated samples are shown in Figure 4.11. Theoretically, the PL emission of the P3HT:PCBM material should be zero, due to the ultrafast charge transfer process from the polymer to the fullerene[24]. Realistically, the PCBM molecules are not so perfectly arranged that they can completely quench the luminescence of P3HT, accounting for the signal observed here. The reduction in the signal strength corresponds to the increasing

radiation dose, but very little change in the linewidth or shifting of the PL peaks are observed.

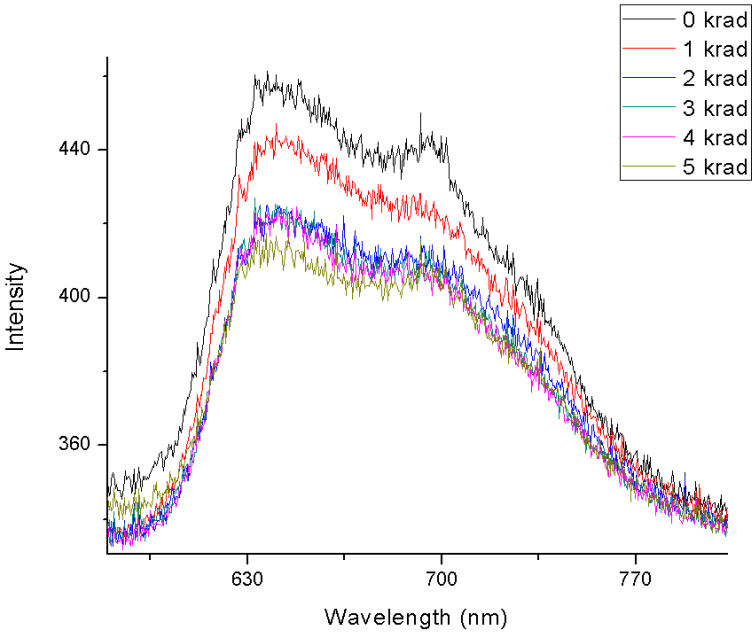

Figure 4.11. Photoluminescence spectra with 490 nm excitation wavelength.

Chapter 5

Discussion

The degradation in the performance of P3HT:PCBM cells is clearly non-trivial. The devices are still functional after the 5 krad radiation dose and there is evidence to suggest some self-recovery of such devices[21]. Degradation of the consitutent materials within these devices has not been well studied either, but there is some knowledge of the behavior of fullerene structures under irradiation and a general understanding of the physical damages to polymers under irradiation.

The results of the conduction, I-TOF, and CELIV measurements show a clear reduction in the device performance with the increasing radiation dose. In the case of I-TOF and CELIV measurements there is a strong decrease in the signal strength, evident of a reduction in the photoexcitations within the active layer or a reduction in the ability of the device to extract current. The former is not so easy to directly measure, but the decrease in the charge carrier mobility within the material is verified by I-TOF and CELIV measurements. The following sections will discuss the possible degradation that occurs within the polymer/fullerene phase and how this degradation will affect device performance.

5.1 Damage to PCBM

Radiation studies on the transport properties of the PCBM molecule are lacking. One must instead consider the changes in properties of the Buckminsterfullerene (C_{60}) under irradiation as analagous to PCBM in order to gain insight. The C_{60} and other carbon systems have been observed under irradiation by electron microscopes for the purposes of studying the formation,

stability, and damage to such materials.

Films composed of fullerenes that are exposed to irradiation by electrons of energy higher than the threshold energy (approximately 100 keV) suffer structural damage due to knock-on displacement of carbon atoms[53, 54]. These vacancies in the fullerene are quickly refilled by other carbon atoms that have been displaced[55]. This effect is most prominent when films of graphite and fullerenes are irradiated due to the high availability of free carbon atoms in the graphite phase. These studies are valid when comparing PCBM to C_{60} because the structure of PCBM is that of a C_{60} molecule with a functional attachment to increase the solubility.

5.2 Damage to P3HT

Conduction in P3HT can occur by charge transport along the polymer backbone, or by adjacent chain interactions. Our P3HT is of the regioregular (RR) configuration, wherein the size, distribution, and alignment of the polymer side chains are tightly controlled. The dominant charge transport mechanism is polaron hoping from chain-to-chain because of the short interchain distance of approximately 3.8 Å [56]. The much better performance of RR-P3HT over the regiorandom (RRa) P3HT is also due to the self-assembly of RR-P3HT into 2-dimensional lamallae, parallel to the substrate, as the solvent evaporates. Figure 5.1 [57] shows the two configurations of P3HT and the 2-dimensional lamallae which form in RR-P3HT.

Creating the device in the layer structure detailed in Chapter 3 is ideal for achieving the highest performance of the P3HT material. This locates the electrical contacts perpendicular to the plane of the 2D lamallae and facilitates the interchain charge hopping[57]. Absorption and photoluminescence experiments have confirmed that RR-P3HT forms this quasi-crystalline structure and has less initial defects than regiorandom-P3HT[56]. The RRa-P3HT exhibits greatly reduced hole mobility due to large disorder in the material which impedes the dominant charge transport mechanism of interchain hopping. The results of the I-V curve measurements show a decrease in short-circuit photocurrent and the FF of the devices with increasing radiation dose. A study of the atmospheric, photo-induced (AM1.5) degradation of P3HT attributes decreases in these parameters to a drop in the P3HT hole mobility[58] resulting from the loss of regioregularity[59]. Radiation ionization of the polymer phase and the subsequent loss of regioregularity is thought to be largely responsible for the overall conductivity degradation observed for the irradiated sam-

ples.

5.2.1 Chain scission and reduced π-conjugation

Chain scission is the breaking of the polymer chain and is brought about by photochemical reactions[60].

A physical alteration such as this will reduce the available conduction pathways for charge carriers and affect the photovoltaic performance in two ways: (1) photoexcitons which do not form so close to a PCBM interface site may not have an energetically favorable pathway to reach the interface and (2) the observed hole mobility of P3HT will be decreased as the contribution of the polymer backbone charge drift to overall charge transport is destroyed by the radiation interaction.

Detrimental chemical reactions in the bulk P3HT are initiated when the samples are exposed to radiation in an oxygen environment. It has been proposed that a singlet oxygen reaction will

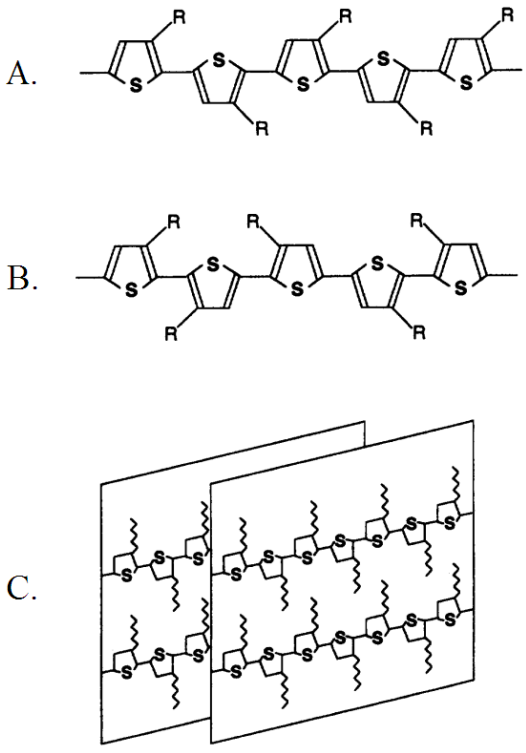

Figure 5.1. Schematic representation of (a) regioregular P3HT, (b) regiorandom P3HT, and (c) the self-assembled, 2D lamallae of RR-P3HT

disrupt the π-conjugation of P3HT[59]. Energy transfer from the triplet excited state of P3HT forms the singlet-O_2. Singlet-O_2 forms an allylic hydroperoxide with polymeric double bonds[61]. Photolysis of the hydroperoxide initiates the chain scission reaction. Degradation of the polymer by this mechanism has been observed for P3HT in both thin films and solutions when exposed to UV-radiation in oxygen[29, 62].

The PL spectra of the material is dependent on the conjugation length of the polymer[63]. Thus, the reduction in the PL intensity with increasing radiation confirms that there is a photooxidation reaction ocurring. The defects introduced into the P3HT structure by the reaction serve to quench the PL emission, as they effectively cause the thermal dissociation of excitons. Experiments with other conjugated polymers confirm that there is an observable decrease in PL efficiency due to the photooxidation reaction[64, 65].

Chapter 6

Conclusions

6.1 Summary of Accomplished Work

In this investigation we have used several electronic and optical measurement techniques to study the performance degradation of novel polymer-based photovoltaic devices. The P3HT:PCBM nanocomposite material is currently one of the highest performing organic photovoltaic systems because it takes advantage of the photo-induced, ultrafast charge transfer process between the donor polymer and acceptor fullerene molecule. The quasi-crystalline arrangement of the PCBM molecules and the self-assembled 2D lamallae of the P3HT facilitates the interchain charge carrier hopping process that yields relatively high mobilities for the device. When exposed to gamma radiation a reduction of the carrier mobility, short-circuit photocurrent, and device fill factor are observed.

The optical measurement of the absorption spectra shows little change before and after the exposure to radiation, revealing that the damage induced by the exposure is not a bulk phenomenon but is highly localized. The photoluminescence spectra shows a decrease in the emission intensity corresponding to an increase in radiation dose. The P3HT phase is responsible for the observed PL emission, and the reduction in the intensity confirms that there is an interaction between the polymer and radiation that introduces defects into the P3HT phase. The defects arise from a photooxidation reaction that causes a reduction in the conjugation length of the polymer—by chain scission or conformational changes (twisting)—and they effectively quench a portion of the photogenerated excitons. Both types of defects detract from the desireable, high-mobility

interchain charge carrier hopping process that dominates charge transport in RR-P3HT, and a decrease in the carrier mobility is thus observed.

6.2 Description of Future Work

There is plenty of future work that can be completed on P3HT:PCBM before such a material can be utilized in radiation environments. Most importantly, it is clear that P3HT is highly susceptible to oxidation effects when radiation exposures are carried out in the ambient environment. A series of experiments can be conducted to study pure P3HT and the role that oxygen plays in the destruction of the device. Packaged samples can be made by utilizing a packed calcium oxide powder and a cover plate affixed with epoxy. These samples could be exposed to radiation through the glass side, and the photoluminescence spectra could still be measured. The experiment would remove the oxidation effects from the damage mechanisms for P3HT and give some detail into the radiation lifetime of the pure material, as destruction of the PL emission essentially means the polymer chains have been reduced to only several units long.

References

[1] Chapin, D., C. S. Fuller, and G. L. Pearson (1954) "A new silicon p-n junction photocell for converting solar radiation into electrical power," *Journal of Applied Physics*, **25**, p. 676.

[2] Blom, P. W., V. D. Mihailetchi, L. J. A. Koster, and D. E. Markov (2007) "Device physics of polymer:fullerene bulk heterojunction solar cells," *Advanced Materials*, **19**, pp. 1551–1556.

[3] Yu, G., J. Gao, J. C. Hummelen, F. Wudl, and A. J. Heeger (1995) "Polymer photovoltaic cells: enhanced efficiencies via a network of internal donor-acceptor heterojunctions," *Science*, **270**, p. 1789.

[4] Debney, B. T. (1979) "A theoretical evaluation and optimization of the radiation resistance of gallium arsenide soar-cell structures," *Journal of Applied Physics*, **50**, p. 7210.

[5] Danilchenko, B., A. Budnyk, L. Shpinar, D. Poplavskyy, and S. E. Zelensky (2008) "1MeV electron irradiation influence on GaAs solar cells performance," *Solar Energy Materials & Solar Cells*, **92**, pp. 1336–1340.

[6] Fleetwood, D. M., P. S. Winokur, and P. E. Dodd (2000) "An overview of radiation effects on electronics in the space telecommunications environment," *Microelectronics Reliability*, **40**(1), pp. 17 – 26.

[7] Pease, R. L., A. H. Johnston, and J. L. Azarewicz (1988) "Radiation testing of semiconductor devices for space electronics," in *Proceedings of the IEEE*, vol. 76, pp. 1510–1526.

[8] Hu, Z., S. He, and D. Yang (2006) "Radiation effects of protons and electrons on backfield silicon solar cells," in *Protection of Materials and Structures from Space Environment: Proceedings of the ICPMSE-6* (J. Kleiman, ed.), difficult to find publishing information for the proceedings.

[9] Bätzner, D. L., A. Romeo, M. Döbeli, K. Weinert, H. Zogg, and A. N. Tiwari (2002) "High energy irradiation properties of CdTe/CdS solar cells," *IEEE*, p. 982.

[10] Budaguan, B. G., A. A. Scherchenkov, A. V. Sizov, and A. B. Grabov (2002) "Investigation of transport mechanism in silicon solar cells after the exploitation in space," *IEEE*, **967**.

[11] Imaizumi, M., T. Takamoto, T. Ohshima, M. Yamaguchi, H. Itoh, and S. Matsuda (2002) "Radiation effects on high-efficiency InGaP/InGaAs/Ge triple-junction solar cells developed for terrestrial use," *IEEE*, p. 990.

[12] Khan, A., M. Yamaguchi, J. C. Bourgoin, and T. Takamoto (2002) "Fundamental understanding of radiation-induced defects in n+ p InGaP solar cells," *IEEE*, p. 1002.

[13] Kurtz, S., R. R. King, K. M. Edmondson, D. J. Friedman, and N. H. Karam (2002) "1-MeV-electron irradiation of GaInAsN cells," *IEEE*, p. 1006.

[14] Weinberg, I., C. K. Swartz, R. E. Hart, and R. L. Statler (1987) *Radiation and temperature effects in gallium arsenide, indium phosphide, and silicon solar cells*, *Tech. rep.*, NASA.

[15] Yamaguchi, M., A. Khan, and N. Dharmarasu (2002) "Consideration on unique radiation-tolerance properties of solar cells made with InP-family," *IEEE*, p. 792.

[16] Yamaguchi, M., C. Uemura, and A. Yamamoto (1984) "Radiation damage in InP single crystal and solar cells," *Journal of Applied Physics*, **55**, p. 1429.

[17] Tonomura, Y., M. Hagino, H. Washio, M. Kaneiwa, T. Saga, O. Anzawa, K. Aoyama, K. Shinozaki, and S. Matsuda (2001) "Development of both-side junction silicon space solar cells," *Solar Energy Materials and Solar Cells*, **66**(1-4), pp. 551 – 558.

[18] Jasenek, A. and U. Rau (2001) "Defect generation in Cu(In,Ga)Se_2 heterojunction solar cells by high-energy electron and proton irradiation," *Journal of Applied Physics*, **90**(2), pp. 650–658.

[19] Shaheen, S. E., R. Radspinner, N. Peyghambarian, and G. E. Jabbour (2001) "Fabrication of bulk heterojunction plastic solar cells by screen printing," *Applied Physics Letters*, **79**(18), pp. 2996–2998.

[20] Brabec, C. J., N. S. Sariciftci, and J. C. Hummelen (2001) "Plastic Solar Cells," *Advanced Functional Materials*, **11-26**, p. 15.

[21] Li, G., Y. Yang, R. A. B. Devine, and C. Mayberry (2008) "Radiation induced damage and recovery in poly(3-hexylthiophene) based polymer solar cells," *Nanotechnology*, **19**, p. 424014.

[22] Zhong, H., Y. Zhao, Y. Li, and Q. Pei (19) "Photoluminescence quenching of conjugated polymer nanocomposites for gamma ray detection," *Nanotechnology*, **2008**, p. 505503.

[23] Hoppe, H. and N. S. Sariciftci (2004) "Organic solar cells: an overview," *Journal of Materials Research*, **19**, p. 1924.

[24] Sariciftci, N. S., L. Smilowitz, A. J. Heeger, and F. Wudl (1992) "Photoinduced electron transfer from a conducting polymer to buckminsterfullerene," *Science*, **258**, p. 1474.

[25] Morel, D. L., A. K. Ghosh, T. Feng, E. L. Stogryn, P. E. Purwin, R. F. Shaw, and C. Fishman (1978) "High-efficiency organic solar cells," *Applied Physics Letters*, **32**, p. 495.

[26] Ghosh, A. K. and T. Feng (1978) "Merocyanine organic solar cells," *Journal of Applied Physics*, **49**, p. 5982.

[27] Günes, S., H. Neugebauer, and N. S. Sariciftci (2007) "Conjugated polymer-based organic solar cells," *Chem. Rev.*, **107**, pp. 1324–1338.

[28] Tang, C. W. (1986) "Two-layer organic photovoltaic cell," *Applied Physics Letters*, **48**, pp. 183–185.

[29] Abdou, M. S. A. and S. Holdcroft (1995) "Solid-state photochemistry of pi-conjugated poly(3-akylthiophenes)," *Canadian Journal of Chemistry*, **73**, pp. 1893–1901.

[30] Dekker, M. (1998) *Handbook of Conducting Polymers*, 2 ed., New York.

[31] McCullough, R. D. (1998) "The chemistry of conducting pholythiophenes," *Advanced Materials*, **10**, p. 93.

[32] Reddinger, J. L. and J. R. Reynolds (1999) *Advances in Polymer Science*, chap. Molecular engineering of pi-conjugated polymers, Springer Berlin / Heidelberg, pp. 57–122.

[33] Nunzi, J.-M. (2002) "Organic photovoltaic materials and devices," *C. R. Physique*, **3**, pp. 523–542.

[34] Brabec, C. J., G. Zerza, G. Cerullo, S. De Silvestri, S. Luzzati, J. C. Hummelen, and S. Sariciftci (2001) "Tracing photoinduced electron transfer process in conjugated polymer/fullerene bulk heterojunctions in real time," *Chemical Physics Letters*, **340**, pp. 232–236.

[35] Wudl, F. (1992) "The chemical properties of buckminsterfullerene (C_{60}) and the birth and infancy of fulleroids," *Accounts of Chemical Research*, **25**(3), pp. 157–161.

[36] Hoppe, H. and N. S. Sariciftci (2006) "Morphology of polymer/fullerene bulk heterojunction solar cells," *Journal of Materials Chemistry*, **16**, pp. 45–61.

[37] Chirvase, D., J. Parisi, J. C. Hummelen, and V. Dyakonov (2004) "Influence of nanomorphology on the photovoltaic action of polymer-fullerene composites," *Nanotechnology*, **15**, pp. 1317–1323.

[38] Schilinsky, P., C. Waldauf, and C. J. Brabec (2002) "Recombination and loss analysis in polythiophene based bulk heterojunction photodetectors," *Applied Physics Letters*, **81**(20), pp. 3885–3887.

[39] Li, G., V. Shrotriya, J. Huang, Y. Yao, T. Moriarty, K. Emery, and Y. Yang (2005) "High-efficiency solution processable polymer photovoltaic cells by self-organization of polymer blends," *Nature Materials*, **4**, p. 864.

[40] Shrotriya, V., J. Ouyang, R. J. Tseng, G. Li, and Y. Yang (2005) "Absorption spectra modification in poly(3-hexylthiophene):methanofullerene blend thin films," *Chemical Physics Letters*, **411**, pp. 138–143.

[41] Shaheen, S. E., C. J. Brabec, N. S. Sariciftci, F. Padinger, T. Fromherz, and J. C. Hummelen (2001) "2.5% Efficient organic plastic solar cells," *Applied Physics Letters*, **78**, pp. 841–843.

[42] Reyes-Reyes, M., K. Kim, and D. L. Carroll (2005) "High-efficiency photovoltaic devices based on annealed poly(3-hexylthiophene) and 1-(3-methoxycarbonyl)-propyl-1-phenyl-(6,6)C_{61} blends," *Applied Physics Letters*, **87**, p. 083506.

[43] Ahn, T., H. Lee, and S.-H. Han (2002) "Effect of annealing of polythiophene derivative for polymer light-emitting diodes," *Applied Physics Letters*, **80**(3), p. 392.

[44] Brown, P. J., D. S. Thomas, A. Köhler, J. S. Wilson, J.-S. Kim, C. M. Ramsdale, H. Sirringhaus, and R. H. Friend (2003) "Effect of interchain interactions on the absorption and emission of poly(3-hexylthiophene)," *Phys. Rev. B*, **67**, p. 064203.

[45] Neugebauer, H., C. Brabec, J. Hummelen, R. Janssen, and N. Sariciftci (1999) "Stability studies and degradation analysis of plastic solar cell materials by FTIR spectroscopy," *Synthetic Metals*, **102**(1-3), pp. 1002 – 1003.

[46] Neugebauer, H., C. Brabec, J. C. Hummelen, and N. S. Sariciftci (2000) "Stability and photodegradation mechanisms of conjugated polymer/fullerene plastic solar cells," *Solar Energy Materials and Solar Cells*, **61**(1), pp. 35 – 42.

[47] Reese, M. O., A. J. Morfa, M. S. White, N. Kopidakis, S. E. Shaheen, G. Rumbles, and D. S. Ginley (2008) "Pathways for the degradation of organic photovoltaic P3HT:PCBM based devices," *Solar Energy Materials & Solar Cells*, **92**, pp. 746–752.

[48] Juška, G., K. Arlauskas, R. Österbacka, and H. Stubb (2000) "Time-of-flight measurements in thin films of regioregular poly(3-hexyl thiophene)," *Synthetic Metals*, **109**(1-3), pp. 173 – 176.

[49] Genevičius, K., R. Österbacka, G. Juška, K. Arlauskas, and H. Stubb (2003) "Separation of fast and slow transport in regiorandom poly(3-hexylthiophene)," *Synthetic Metals*, **137**, pp. 1407–1408.

[50] Österbacka, R., G. Juška, K. Arlauskas, and H. Stubb (1997) "Time-of-flight measurements in Langmuir-Blodgett films of poly(3-hexylthiophene)," *SPIE*, **3145**, pp. 389–394.

[51] Juška, G., K. Genevičius, M. Viliunas, K. Arlauskas, H. Stuchlíková, A. Fejfar, and J. Kočka (2000) "New method of drift mobility evaluation in [mu]c-Si:H, basic idea and comparison with time-of-flight," *Journal of Non-Crystalline Solids*, **266-269**(Part 1), pp. 331 – 335.

[52] Pivrikas, A., N. S. Sariciftci, G. Juška, and R. Österbacka (2007) "A review of charge transport and recombination in polymer/fullerene organic solar cells," *Progress in Photovoltaics: Research and Applications*, **15**, pp. 667–696.

[53] Banhart, F. (2002) "Structural transformations in carbon nanoparticles induced by electron irradiation," *Physics of the Solid State*, **44**, pp. 399–404.

[54] Dmytrenko, O. P., N. P. Kulish, N. Belyi, Y. I. Prylutskyy, L. V. Poperenko, V. S. Stashchuk, V. G. Poroshin, E. L. Pavlenko, V. V. Shlapatskaya, H. Bernas, and P. Scharff (2006) "Dose dependences of the optical properites of fullerene films subjected to the electron irradiation," *Thin Solid Films*, **495**, pp. 365–367.

[55] Füller, T. and F. Banhart (1996) "In situ observation of the formation and stability of single fullerene molecules under electron irradiation," *Chemical Physics Letters*, **254**, pp. 372–378.

[56] Jiang, X., R. Österbacka, O. Korovyanko, C. P. An, B. Horovitz, R. A. Janssen, and Z. V. Vardeny (2002) "Spectroscopic studies of photoexcitations in regioregular and regiorandom polythiophene films," *Advanced Functional Materials*, **12**, pp. 587–597.

[57] Cornil, J., D. Beljonne, J.-P. Calbert, and J.-L. Brédas (2001) "Interchain interactions in organic pi-conjugated materials: impact on electronic structure, optical response, and charge transport," *Advanced Materials*, **13**(14), pp. 1053–1067.

[58] Chang, Y.-M., W.-F. Su, and L. Wang (2008) "Influence of photo-induced degradation on the optoelectronic properties of regioregular poly(3-hexylthiophene)," *Solar and Energy Materials & Solar Cells*, **92**, pp. 761–765.

[59] Manceau, M., A. Rivaton, J.-L. Gardette, S. Guillerez, and N. Lematre (2009) "The mechanism of photo- and thermooxidation of poly(3-hexylthiophene) (P3HT) reconsidered," *Polymer Degradation and Stability*, **94**, pp. 898–907.

[60] Marciniak, S., X. Crispin, K. Uvdal, M. Trzcinksi, J. Birgerson, L. Groenendaal, F. Louwet, and W. R. Salaneck (2004) "Light induced damage in poly(3,4-ethylenedioxythiophene) and its derivatives studied by photoeletron spectroscopy," *Synthetic Metals*, **141**, pp. 67–73.

[61] Holdcroft, S. (1991) "Photochain scission of the soluble electronically conducting polymer: poly(3-hexylthiophene)," *Macromolecules*, **24**, pp. 2119–2121.

[62] Abdou, M. S. A. and S. Holdcroft (1993) "Mechanisms of photodegradation of poly(3-akylthiophenes) in solution," *Macromolecules*, **26**(11), pp. 2954–2962.

[63] Zapunidi, S. A. and D. Y. Paraschuk (2008) "Photoluminescence quenching through resonant energy transfer in blends of conjugated polymer with low-molecular acceptor," *Journal of Experimental and Theoretical Physics*, **107**, pp. 1079–1089.

[64] Wang, Y.-h., Y.-j. Peng, Y.-q. Mo, Y.-q. Yang, and X.-x. Zheng (2008) "Analysis on the mechanism of photoluminescence quenching in pi-conjugated polymers in photo-oxidation process with broadband transient grating," *Applied Physics Letters*, **93**, p. 231902.

[65] Yan, M., L. J. Rothberg, F. Papadimitrakopoulos, M. E. Galvin, and T. M. Miller (1994) "Defect quenching of conjugated polymer luminescence," *Physical Review Letters*, **73**(5), pp. 744–747.